FeTe_{0.55}Se_{0.45}: A multiband superconductor in the clean and dirty limit

C. C. Homes, Y. M. Dai, J. S. Wen, Z. J. Xu, and G. D. Gu

Phys. Rev. B **91**, 144503 — Published 10 April 2015

DOI: 10.1103/PhysRevB.91.144503

$FeTe_{0.55}Se_{0.45}$: a multiband superconductor in the clean and dirty limit

C. C. Homes,* Y. M. Dai,† J. S. Wen, Z. J. Xu, and G. D. Gu
Condensed Matter Physics and Materials Science Department,
Brookhaven National Laboratory, Upton, New York 11973, USA
(Dated: March 23, 2015)

The detailed optical properties of the multiband iron-chalcogenide superconductor $FeTe_{0.55}Se_{0.45}$ have been reexamined for a large number of temperatures above and below the critical temperature $T_c = 14$ K for light polarized in the *a*-*b* planes. Instead of the simple Drude model that assumes a single band, above T_c the normal-state optical properties are best described by the two-Drude model that considers two separate electronic subsystems; we observe a weak response ($\omega_{p,D;1} \simeq 3000$ cm^{-1}) where the scattering rate has a strong temperature dependence ($1/\tau_{D,1} \simeq 32$ cm^{-1} for $T \gtrsim T_c$), and a strong response ($\omega_{p,D;2} \simeq 14\,500$ cm^{-1}) with a large scattering rate ($1/\tau_{D,2} \simeq 1720$ cm^{-1}) that is essentially temperature independent. The multiband nature of this material precludes the use of the popular generalized-Drude approach commonly applied to single-band materials, implying that any structure observed in the frequency dependent scattering rate $1/\tau(\omega)$ is spurious and it cannot be used as the foundation for optical inversion techniques to determine an electron-boson spectral function $\alpha^2F(\omega)$. Below T_c the optical conductivity is best described using two superconducting optical gaps of $2\Delta_1 \simeq 45$ and $2\Delta_2 \simeq 90$ cm^{-1} applied to the strong and weak responses, respectively. The scattering rates for these two bands are vastly different at low temperature, placing this material simultaneously in both clean and dirty limit. Interestingly, this material falls on the universal scaling line initially observed for the cuprate superconductors.

PACS numbers: 74.25.Gz, 74.70.Xa, 78.30.-j

I. INTRODUCTION

The discovery of superconductivity in the iron-based materials[1–3] with maximum superconducting transition temperatures of $T_c \sim 55$ K achieved through rare-earth substitution[4] has prompted a tremendous amount of research into the structural and electronic properties of this class of materials,[5] not only to ascertain the nature of the superconductivity but also to find a path to higher transition temperatures. Recently, attention has focused on the iron-chalcogenide materials; these materials are structurally simple, consisting only of layers of $Fe_2(Se/Te)_2$ tetrahedra.[3] Nearly stoichiometric $Fe_{1+\delta}Te$ undergoes a first-order magnetic and structural transition[6–8] from a tetragonal, paramagnetic state to a monoclinic, antiferromagnetic state at $T_N \simeq 68$ K, but remains metallic down to the lowest measured temperature. Superconductivity has been observed at ambient pressure in FeSe with $T_c = 8$ K,[3] increasing to $T_c \simeq 37$ K under pressure.[9] The substitution of Te with Se in $FeTe_{1-x}Se_x$ suppresses the structural and magnetic transition and establishes superconductivity over a broad range of compositions[10,11] with the critical temperature reaching a maximum value[12–18] of $T_c \simeq 14$ K for $x \simeq 0.45$; enhanced T_c's have been reported in thin films.[19,20]

Electronic structure calculations reveal a multiband material with three hole-like bands at the origin and two electron-like bands at the corners of the Brillouin zone,[21] a Fermi surface topology common to many of the iron-based superconductors. Angle resolved photoemission spectroscopy (ARPES) typically identify most of these bands.[22–26] Multiple isotropic superconducting energy gaps $\Delta \simeq 2-4$ meV have been observed,[27,28] and there is also evidence for an anisotropic superconducting gap on one of the hole surfaces.[29] Despite being a multiband material with more than one type of free carrier, these materials are poor metals.[16,17] The optical properties in the Fe-Te/Se (*a*-*b*) planes of $FeTe_{0.55}Se_{0.45}$ reveal a material that appears to be almost incoherent at room temperature but that develops a metallic character just above T_c. Below T_c the emergence of a superconducting state is seen clearly in the in-plane optical properties.[30–32] Perpendicular to the planes (*c* axis) the transport appears incoherent and displays little temperature dependence; below T_c no evidence of a gap or a condensate is observed.[33]

In this work the detailed optical properties of $FeTe_{0.55}Se_{0.45}$ in the *a*-*b* planes are examined at a large number of temperatures in the normal state and analyzed using the two-Drude model,[34,35] which considers two electronic subsystems rather than a single electronic band; this approach has been successfully applied to thin films of this material.[32] The single-band approach was used in a previous study of this material and was the basis for the application of the generalized Drude model;[30] however, we demonstrate that the multiband nature of this material precludes the use of the generalized Drude model. The two-Drude model reveals a relatively weak Drude component ($\omega_{p,D;1} \simeq 3000$ cm^{-1}) with a small, strongly temperature dependent scattering rate at low temperature ($1/\tau_{D,1} \simeq 32$ cm^{-1}), and a much stronger Drude component where the strength ($\omega_{p,D;2} \simeq 14\,500$ cm^{-1}) and the scattering rate ($1/\tau_{D,2} \simeq 1720$ cm^{-1}) display little or no temperature dependence. In the superconducting state the optical conductivity is reproduced quite well by introducing isotropic superconducting gaps of $2\Delta_1 \simeq 45$ cm^{-1} on the broad Drude response, and $2\Delta_2 \simeq 90$ cm^{-1} on the narrow Drude component; no fitting is performed. Comparing gaps and the scattering rates, we note that $1/\tau_{D,1} \lesssim 2\Delta_1(2\Delta_2)$, placing this close to the clean limit, while $1/\tau_{D,2} \gg 2\Delta_1(2\Delta_2)$, which is in the dirty limit; as a result, this multiband material is simultaneously in both the clean and dirty limit. The decomposition of the superconducting response into two bands allows the different contributions to the superfluid density to be examined. While the experimentally-determined value and the clean-limit contribution falls on the universal scaling line for the high-temperature superconductors[36] in the region of the underdoped cuprates, the dirty-limit contribution falls very close to the scaling line predicted for a dirty-limit BCS superconductor.[37] New results for this scaling relation indicate that it will be valid in both the clean and dirty limit,[38] which explains how this material can satisfy both conditions and still fall on the scaling line.

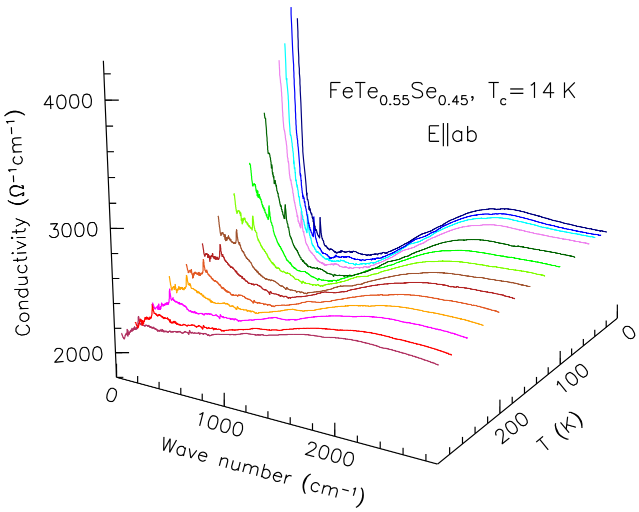

FIG. 1. (Color online) The real part of the in-plane optical conductivity of $FeTe_{0.55}Se_{0.45}$ for a large number of temperatures in the normal state in the far and mid-infrared region, showing the rapid emergence with decreasing temperature of a Drude-like response at low frequency.

II. EXPERIMENT

A mm-sized single crystal of $FeTe_{0.55}Se_{0.45}$ was cleaved from a piece of the sample used in the original optical study[30] revealing a flat, lustrous surface along the Fe-Te/Se (*a*-*b*) planes; this crystal has a critical temperature of $T_c = 14$ K with a transition width of $\simeq 1$ K. The reflectance has been measured at a near-normal angle of incidence for a large number of temperatures (16) above and below T_c over a wide frequency range (~ 3 meV to 3 eV) for light polarized in the *a*-*b* planes using an *in situ* overcoating technique.[39] The complex optical properties have been determined from a Kramers-Kronig analysis of the reflectance,[40] the details of which have been previously described.[30]

III. RESULTS AND DISCUSSION

A. Normal state

The optical conductivity in the far and mid-infrared regions is shown for a variety of temperatures above T_c in the waterfall plot in Fig. 1. At room temperature, the conductivity is essentially flat over the entire frequency region. The optical properties can be described using a simple Drude-Lorentz model for the dielectric function:

$$\tilde{\epsilon}(\omega) = \epsilon_\infty - \frac{\omega_{p,D}^2}{\omega^2 + i\omega/\tau_D} + \sum_j \frac{\Omega_j^2}{\omega_j^2 - \omega^2 - i\omega\gamma_j}, \quad (1)$$

where ϵ_∞ is the real part at high frequency, $\omega_{p,D}^2 = 4\pi n e^2/m^*$ and $1/\tau_D$ are the square of the plasma frequency and scattering rate for the delocalized (Drude) carriers, respectively, and n and m^* are the carrier concentration and effective mass. In the summation, ω_j, γ_j and Ω_j are the position, width, and strength of the jth vibration or bound excitation. The complex conductivity is $\tilde{\sigma}(\omega) = \sigma_1 + i\sigma_2 = -i\omega[\tilde{\epsilon}(\omega) - \epsilon_\infty]/60$ (in units of Ω^{-1}cm^{-1}). The Drude response is simply a Lorentzian centered at zero frequency with a full-width at half maximum of $1/\tau_D$. The scattering rate typically decreases with temperature, leading to a narrowing of the Drude response and the transfer of spectral weight from high to low frequency, where the spectral weight is the area under the conductivity curve, $N(\omega, T) = \int_0^\omega \sigma_1(\omega')\, d\omega'$. As Fig. 1 indicates, while there is no clear free-carrier response at room temperature, there is a rapid formation of a Drude-like response below about 200 K with a commensurate transfer of spectral weight from high to low frequency below $\simeq 2000$ cm^{-1}.

The optical conductivity may be modeled quite well with only a single Drude term; however, this is only possible if an extremely low-frequency Lorentzian oscillator ($\omega_0 \lesssim 3$ meV) is included. While low-energy interband transitions are expected for this class of materials,[41] they are not expected to fall below $\simeq 30$ meV, well above the low-frequency oscillator required to fit the data using this approach. This suggests that a multiband system like $FeTe_{0.55}Se_{0.45}$ is more correctly described by a two-Drude model[34,35] in which the electronic response is modeled as two separate, uncorrelated electronic subsystems rather than a single dominant band. Using this approach, the second term in Eq. (1) becomes a summation in which the plasma frequency and the scattering rate are now indexed over the total number of bands under consideration (two in this case). Both the real and imaginary parts of the conductivity are fit simultaneously using a non-linear least-squares method, which allows very broad features to be fit more reliably than fitting to just the real part

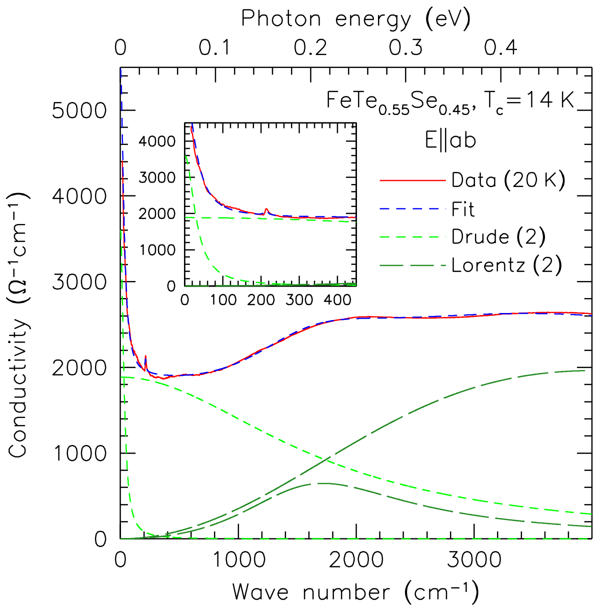

FIG. 2. (Color online) The Drude-Lorentz model fit to the real part of the optical conductivity of $FeTe_{0.55}Se_{0.45}$ at 20 K for light polarized in the *a*-*b* planes for two Drude components and two Lorentz oscillators. The inset shows the linear combination of the two Drude components in the low frequency region; the sharp structure at $\simeq 204$ cm^{-1} is the normally infrared-active E_u mode.[30]

of the optical conductivity alone.

The result of the fit to the data at 20 K is shown in Fig. 2, revealing two distinct Drude components; a narrow response with $\omega_{p,D;1} \simeq 2630$ cm^{-1} and $1/\tau_{D,1} \simeq 32$ cm^{-1}, and a much broader and stronger component with $\omega_{p,D;2} \simeq 14\,110$ cm^{-1} and $1/\tau_{D,2} \simeq 1770$ cm^{-1}. These values are consistent with the results from the two-Drude analysis performed on $FeTe_{0.5}Se_{0.5}$ thin films.[32] The structure in the mid-infrared region is described by two oscillators centered at $\omega_1 \simeq 1720$ cm^{-1} and $\omega_2 \simeq 4010$ cm^{-1}; other high-frequency oscillators have been included to describe the optical conductivity in the near-infrared and visible regions, but they are not shown in this plot.

It is not immediately obvious if the narrow Drude component originates from the electron or the hole pockets. In a previous study of the non-superconducting parent compound $Fe_{1.03}Te$, the weak Drude-like feature at high temperature and the the rapid increase of the low-frequency conductivity below the magnetic and structural transition at $T_N \simeq 68$ K was associated with the closing of the pseudogap on the electron pocket.[42,43] While the scattering rate on the electron pocket in $Fe_{1.03}Te$ was observed to be about 6 meV at low temperature, it also displayed relatively little temperature dependence, whereas in the current study the pocket with the a scattering rate about 4 meV at 20 K shows considerable temperature dependence. In ARPES studies of iron-arsenic superconductors, small scattering rates ($\simeq 3$ meV) have been observed on both the electron and hole pockets at low temperature,[44] which is consistent with the observation that electron and hole mobilities are similar at low temperature in $FeTe_{0.5}Se_{0.5}$, unlike $Fe_{1+\delta}Te$ where the electron mobility is much larger than that of the holes below T_N (Ref. 45). While it is tempting to associate the small scattering rate with an electron pocket, we can not make any definitive statements at this point.

The two-Drude model has been used to fit the real and imaginary parts of the optical conductivity in the normal state for $T > T_c$; the temperature dependence of the plasma frequencies and the scattering rates for the narrow and broad components are shown in Fig. 3. The fit to the optical conductivity at 20 K, and at low temperatures in general, is unambiguous due to the narrow Drude term; as a result, both the plasma frequencies and the scattering rates may be fit simultaneously. As Fig. 3(a) indicates, at low temperature the plasma frequency for the broad component displays little temperature dependence, while the plasma frequency for the narrow Drude component decreases slightly just above T_c. At low temper-

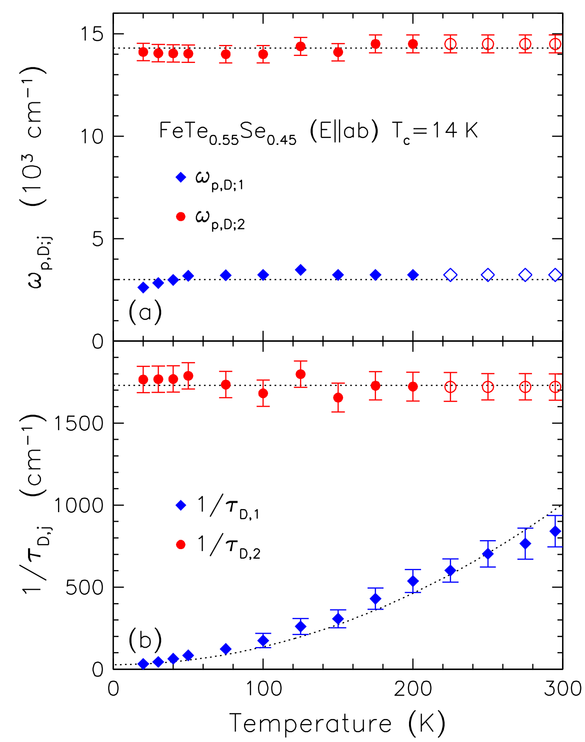

FIG. 3. (Color online) The two-Drude model fit to the optical conductivity yielding the temperature dependence of the (a) plasma frequencies $\omega_{p,D;j}$ and (b) scattering rates $1/\tau_{D,j}$ for the narrow (diamonds) and broad (circles) Drude components in $FeTe_{0.55}Se_{0.45}$ for $T > T_c$. The filled symbols indicate fitted parameters, while the open symbols indicate that the parameter held fixed to a constant value. Where error bars are not shown, the error is roughly the size of the symbol. The dotted lines are drawn as a guide for the eye.

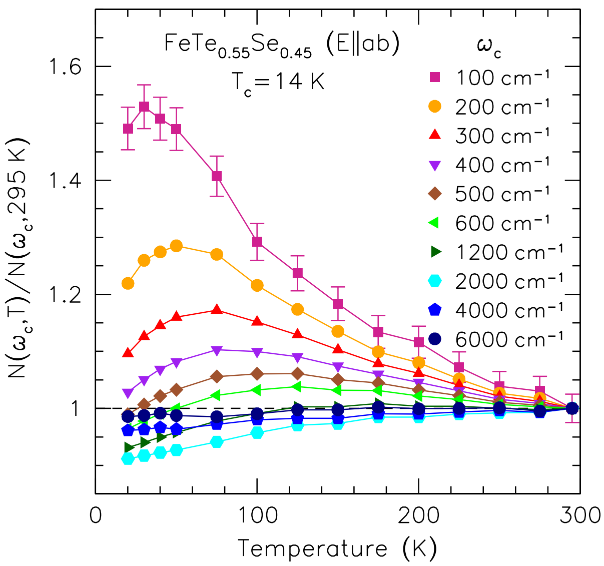

FIG. 4. (Color online) The temperature dependence of the spectral weight normalized to the value at 295 K for a variety of choices for the cut-off frequency ω_c; the estimated error is indicated for the $\omega_c = 100$ cm^{-1} points. Smaller values of ω_c result in a strong temperature dependence; however, within the confidence limits of the experiment, for $\omega_c \gtrsim 4000$ cm^{-1} there is effectively little or no temperature dependence.

atures, the scattering rate for the broad component also displays little temperature dependence, whereas the scattering rate for the narrow component increases quickly with temperature, until by 200 K it has increased by a factor of $\simeq 20$. At high temperature, the presence of two broad Drude terms makes the fit to the now relatively featureless complex conductivity more challenging. As a result, above 200 K the fit is constrained to only the scattering rate for the narrow Drude term; both plasma frequencies and the scattering rate for the broad Drude term are held fixed. This is indicated in Fig. 3 by the solid symbols (fitted parameters), and the open symbols (fixed parameters). Using these constraints, the scattering rate for the narrow Drude term continues to increase until at room temperature $1/\tau_{D,1} \simeq 840$ cm^{-1}, about half the value of the scattering rate observed for the other Drude component. The dotted line shown in Fig. 3 for $1/\tau_{D,1}$ has the quadratic form that would be expected for a Fermi liquid; however, below 100 K the data may be fit equally well by a straight line, making it difficult to draw any conclusions about the nature of the transport on this pocket.

Returning to the evolution of the conductivity in the normal state, it is clear from Fig. 1 that the growth of the low-frequency Drude component is accompanied by the loss of spectral weight throughout much of the infrared region; however, it is important note that these changes occur on top of a large background conductivity that originates from the strong Drude component and several mid-infrared absorptions. To estimate the energy scale over which this transfer takes place, the normalized spectral weight $N(\omega_c, T)/N(\omega_c, 295\,\mathrm{K})$ is plotted in Fig. 4 for a variety of choices for the cut-off frequency, ω_c. Small values of ω_c result in a strong temperature dependence. Normally, larger values of ω_c would eventually result in a temperature-independent curve with a value of unity; however, before this occurs the ratio is first observed to drop below unity for $\omega_c \simeq 600$ cm^{-1} before finally adopting the expected form for $\omega_c \gtrsim 4000$ cm^{-1}. We speculate that this is in response to the reduction of the plasma frequency of the narrow Drude component at low temperature resulting in a transfer of spectral weight from a coherent to an incoherent response at high frequency. This effect has in fact been predicted in the iron-based materials and is attributed to Fermi surface reduction due to many body effects.[46] Finally, we remark that while the redistribution of spectral weight in the parent compound $Fe_{1.03}Te$ below T_N is due to the closing of the pseudogap on the electron pocket in that material,[42,43] in the present case it is due to the slight decrease in the plasma frequency and the dramatic decrease in the scattering rate of the narrow Drude component at low temperature.

B. Generalized Drude model

Beyond the two-component Drude-Lorentz and the two-Drude approaches for modeling the optical conductivity, there is a third approach, the generalized Drude model. This latter approach is commonly used to describe the normal state of the cuprate materials where only a single band crosses the Fermi level, and is referred to as a single component model. The optical conductivity of the cuprates is similar to that of $FeTe_{0.55}Se_{0.45}$; typically, just above T_c, there is a narrow Drude-like response that gives way to a flat, incoherent mid-infrared component, resulting in a kink-like feature in the optical conductivity.[47–49] This kink is attributed to a strongly-renormalized scattering rate due to electron-boson coupling, and is is described in the generalized Drude model through a frequency-dependent scattering rate and effective mass,[50,51]

$$\frac{1}{\tau(\omega)} = \frac{\omega_p^2}{4\pi} \mathrm{Re}\left[\frac{1}{\tilde{\sigma}(\omega)}\right] \tag{2}$$

and

$$\frac{m^*(\omega)}{m_e} = \frac{\omega_p^2}{4\pi\omega} \mathrm{Im}\left[\frac{1}{\tilde{\sigma}(\omega)}\right], \tag{3}$$

where m_e is the bare mass, $m^*(\omega)/m_e = 1 + \lambda(\omega)$ and $\lambda(\omega)$ is a frequency-dependent electron-boson coupling constant. The frequency-dependent scattering rate is the basis for optical inversion methods to calculate the electron-boson spectral function.[52,53] However, concerns have been raised over the effect of the low-energy interband transitions on the scattering rate,[54] and more

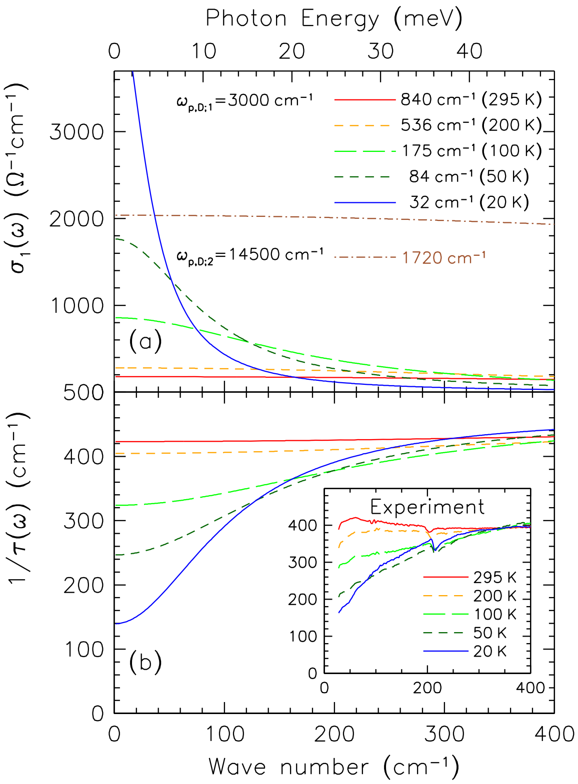

FIG. 5. (Color online) (a) The optical conductivity for the temperature-independent broad, strong Drude component (dot-dash line), and the weaker Drude component (solid and dashed lines) that displays a strongly temperature-dependent scattering rate. (b) The frequency-dependent scattering rate calculated from the two-Drude model. Inset: the experimentally-determined $1/\tau(\omega)$.

generally, the multiband nature of the iron pnictide and iron selenide materials presents a major difficulty for this type of analysis. To illustrate this point, we consider the complex dielectric function for a two Drude model. The plasma frequency for the weak component has been taken to be with $\omega_{p,D;1} \simeq 3000$ cm^{-1}; initially the scattering rate is quite broad with $1/\tau_{D,1} \simeq 840$ cm^{-1} at 295 K, but as Fig. 3 indicates it decreases rapidly with temperature to $1/\tau_{D;1} \simeq 32$ cm^{-1} at 20 K. The optical conductivity at these temperatures, as well as 200, 100, and 50 K, are shown in Fig. 5(a) as the various lines. In addition, a broad, strong Drude component with $\omega_{p,D;2} \simeq 14\,500$ cm^{-1} and $1/\tau_{D,2} \simeq 1720$ cm^{-1} is shown in Fig. 5(a) as a dash-dot line; this component is temperature independent. From these two Drude responses a temperature-dependent complex dielectric function is constructed and the frequency-dependent scattering rate is calculated from Eq. (2) using a somewhat arbitrary value of $\omega_p \simeq 7500$ cm^{-1}; the result is shown in Fig. 5(b). The actual experimental values are shown in the inset using values of $\omega_p \simeq 6700 - 7300$ cm^{-1}, where ω_p has been chosen so that the values for the scattering rate are roughly the same at 400 cm^{-1}. At 295 K, where the scattering rates are broad, $1/\tau(\omega)$ displays little or no frequency dependence, and the same can be said of the result at 200 K; this type of response would be expected from a simple Drude model with only a single component. This trend does not continue; by 100 K the scattering rate has developed strong frequency dependence and by 20 K the scattering rate has a linear frequency dependence over much of the low-frequency region. In a previous single-component analysis of this material, this $1/\tau(\omega) \propto \omega$ behavior was taken as evidence for electronic-correlations.[30] However, the multiband nature of this material indicates that the linear-frequency dependence observed in $1/\tau(\omega)$ is simply a consequence of having more than one Drude component. As a result, unless the system has been heavily doped into a regime where it is either purely electron or hole doped, then the single-component, generalized-Drude approach should be avoided. It should also not be used as a basis for optical-inversion techniques used to calculate the electron-boson spectral function.

C. Superconducting state

1. *Superfluid density*

While the optical conductivity in the normal state in Fig. 1 shows the development of a strong Drude-like component at low temperature, upon entry into the superconducting state there is a dramatic suppression of the low-frequency conductivity and a commensurate loss of spectral weight, shown in Fig. 6(a). The loss of spectral weight is associated with the formation of a superconducting condensate, whose strength may be calculated from the Ferrell-Glover-Tinkham (FGT) sum rule:[55,56]

$$\int_{0^+}^{\omega_c} [\sigma_1(\omega, T \gtrsim T_c) - \sigma_1(\omega, T \ll T_c)]\, d\omega = \omega_{p,S}^2/8, \quad (4)$$

or $\omega_{p,S}^2 = 8\,[N_n(\omega_c, T \gtrsim T_c) - N_s(\omega_c, T \ll T_c)]$, where ω_c is chosen so that the integral converges and $\omega_{p,S}^2 = 4\pi n_s e^2/m^*$ is the superconducting plasma frequency. The superfluid density is $\rho_{s0} \equiv \omega_{p,S}^2$. The evolution of the spectral weight for N_n and N_s are shown in Fig 6(b). It is apparent from Fig. 6(a) that most of the changes in the spectral weight occur below $\simeq 100$ cm^{-1}, so it is therefore not surprising that the expression for $\omega_{p,S}^2$ has converged for $\omega_c \simeq 120$ cm^{-1}. The sum rule yields $\omega_{p,S} \simeq 3280 \pm 200$ cm^{-1}, from which an effective penetration depth can be calculated, $\lambda_0 = 4850 \pm 300$ Å, slightly smaller than the result obtained in the previous optical study,[30] and in good agreement with values of $\lambda_0 \simeq 4300 - 5600$ Å observed in materials with similar composition measured using several different methods.[57–60] In a previous single-band interpretation of the optical conductivity of this material, it was noted that $\omega_{p,S} \ll \omega_{p,D}$, suggesting that only small portion of the free carriers collapsed into the condensate below T_c and that this material was therefore not in the clean limit. However, the multiband nature of this compound results in a more complicated picture where this statement is only partially true.

2. *Multiband superconductor*

The complex optical conductivity shown in Fig. 6(a) is reproduced in Fig. 7(a); as previously noted, below T_c most of the transfer of spectral weight occurs below $\simeq 120$ cm^{-1}, setting a naïve energy scale for the maximum value of the superconducting energy gap. In addition to the general suppression of the optical conductivity below 120 cm^{-1}, there is also a shoulder at $\simeq 60$ cm^{-1}, suggesting more than one energy scale for superconductivity in this material.[61] In the previous work where a single-band interpretation was employed,[30] the optical conductivity was reproduced reasonably well by using a Mattis-Bardeen formalism for the contribution from the gapped excitations.[40,62] The Mattis-Bardeen approach assumes that $l \lesssim \xi_0$, where the mean-free path $l = v_F\tau$

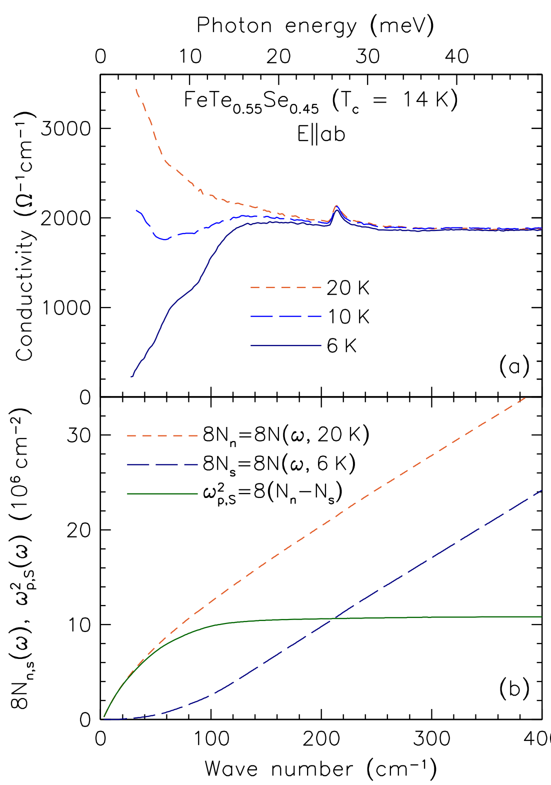

FIG. 6. (Color online) (a) The real part of the optical conductivity for $FeTe_{0.55}Se_{0.45}$ for light polarized in the a-b planes just above T_c at 20 K, and at two temperatures below T_c. Note the strong suppression of the low-frequency conductivity for $T \ll T_c$. (b) The spectral weight in the normal state, $N_n(\omega, T \gtrsim T_c)$ and in the superconducting state, $N_s(\omega, T \ll T_c)$; the expression for $\omega^2_{p,S}$ converges by $\omega \simeq 150$ cm^{-1}.

(v_F is the Fermi velocity), and the coherence length is $\xi_0 = \hbar v_F/\pi\Delta_0$ for an isotropic superconducting gap Δ_0; this may also be expressed as $1/\tau \gtrsim 2\Delta_0$. The best result was obtained by using two isotropic superconducting energy gaps of $2\Delta_1 = 40$ cm^{-1} and $2\Delta_2 = 83$ cm^{-1}, where a moderate amount of disorder-induced scattering was introduced.[30] However, in the two-Drude model, the amount of scattering in each band is dramatically different, $1/\tau_{D,1} \ll 1/\tau_{D,2}$. To model the data, we use the values for the plasma frequencies and the scattering rates just above T_c at 20 K, shown in Fig. 3, for the two different bands; the two isotropic superconducting energy gaps are taken to be $2\Delta_1 = 45$ cm^{-1} and $2\Delta_2 = 90$ cm^{-1}. The contribution from each of the gapped excitations is then calculated. We emphasize at this point that no fitting is employed and that the parameters are not refined.

The solid line in Fig. 7(b) shows the normal-state conductivity for $\omega_{p,D;1} = 2600$ cm^{-1} and $1/\tau_{D,1} = 32$ cm^{-1} for $T \gtrsim T_c$, while dashed lines denote the contributions from the gapped excitations from $2\Delta_1$ and $2\Delta_2$ for $T \ll T_c$. Below the superconducting energy gap the conductivity is zero and there is no absorption, while above the gap there is a rapid onset of the conductivity, which then joins the normal-state value at higher energies. Using the FGT sum rule in Eq. (4) we estimate $\omega_{p,S} \simeq 2150$ cm^{-1} for the lower gap and $\omega_{p,S} \simeq 2300$ cm^{-1} for the upper gap, indicating that about $70-80\%$ of the free carriers collapse into the condensate for $T \ll T_c$. This is consistent with the observation that $1/\tau_{D,1} \lesssim 2\Delta_1, 2\Delta_2$, placing this material in the moderately-clean limit. It has been remarked that for a single-band material in the clean limit the opening of a superconducting energy gap may be difficult to observe because the small normal-state scattering rate can lead to a reflectance that is already close to unity, thus the increase in the reflectance below T_c for $\omega \lesssim 2\Delta$ is difficult to observe.[63] However, this is a multiband material in which the overall superconducting response arises from the gapping of several bands, some of which are not necessarily in the clean limit, discussed below.

The same procedure is carried out for the second band in Fig. 7(c) for $\omega_{p,D;2} = 14\,500$ cm^{-1} and $1/\tau_{D,2} = 1720$ cm^{-1}. Here, the normal-state conductivity is nearly flat in the low-frequency region. For $T \ll T_c$, the conductivity is once again zero below the superconducting energy gap; however, unlike the previous case the onset of conductivity above the gap now takes place much more slowly. In addition, the curves only merge with the normal-state values at energies well above the values for the superconducting gaps. From the FGT sum rule, we estimate $\omega_{p,S} \simeq 2740$ cm^{-1} for the lower gap and $\omega_{p,S} \simeq 3670$ cm^{-1} for the upper gap, indicating that about $3-6\%$ of the free carriers collapse into the condensate for $T \ll T_c$. This is consistent with the observation that $1/\tau_{D,2} \gg 2\Delta_1, 2\Delta_2$, placing this material in the dirty limit. Thus, as a consequence of the multiband nature of this material, it can coexist in both the clean and dirty limit at the same time; we speculate that this

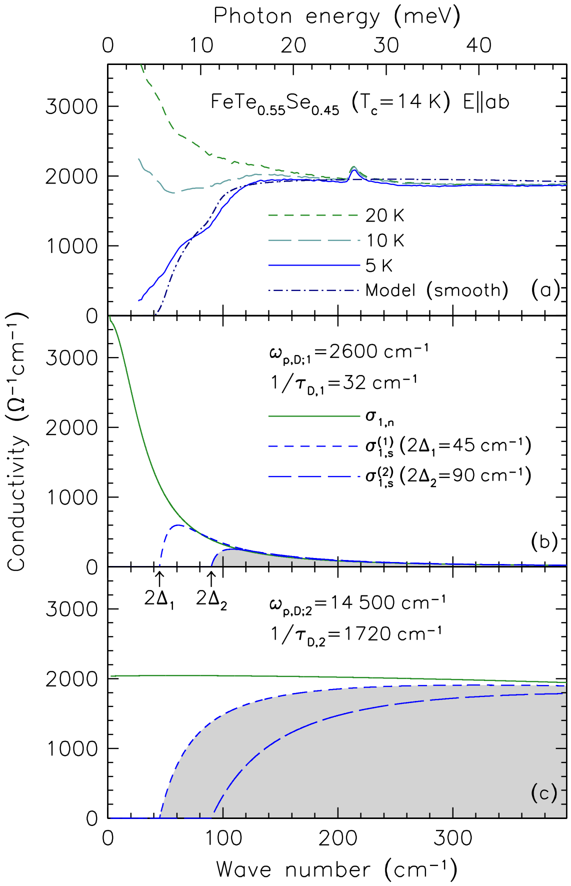

FIG. 7. (Color online) (a) The real part of the optical conductivity for $FeTe_{0.55}Se_{0.45}$ for light polarized in the *a*-*b* planes just above T_c at 20 K, and at two temperatures below T_c. The dash-dot line models the smoothed contribution to the conductivity from the gapped excitations described in the discussion. (b) The real part of the optical conductivity for a Drude model with $\omega_{p,D;1} = 2600$ cm^{-1} and $1/\tau_{D,1} = 32$ cm^{-1} (solid line), and the contribution from the gapped excitations for $T \ll T_c$ with superconducting gaps of $2\Delta_1 = 45$ cm^{-1} and $2\Delta_2 = 90$ cm^{-1} (dashed lines). (c) The same set of calculations for $\omega_{p,D;2} = 14\,500$ cm^{-1} and $1/\tau_{D,2} = 1720$ cm^{-1}.

condition is likely fulfilled in many (if not all) of the iron-based superconductors.

While we have considered the effects of different sizes of superconducting energy gaps on the different bands, only a single isotropic gap is associated with each pocket. In order to reproduce the data in Fig. 7(a), different combinations were considered. The best choice is a linear combination of the large gap $(2\Delta_2)$ applied to the narrow Drude response in Fig. 7(b) and the small $(2\Delta_1)$ gap applied to the broad Drude response in Fig 7(c), indicated by the shaded regions; this line has been smoothed and is shown as the dash-dot line in Fig. 7(a), which manages to reproduce the data quite well. This is somewhat surprising for two reasons. First, the curve has not been refined in any way, and second, this is a simple superposition of two single-band BCS models and not a more sophisticated two-band model of superconductivity that considers both intraband as well as interband pairing.[64–66] On the other hand, since this approach appears to work rather well, we speculate that the large difference in the scattering rates in the two bands allows for this simpler interpretation. Taking the contributions for the superconducting plasma frequencies from the two bands, $\omega_{p,S;1} \simeq 2300$ cm^{-1} from the narrow band and $\omega_{p,S;2} \simeq 2740$ cm^{-1} from the broad band; the strength of the condensate may be estimated by adding the two in quadrature, $\omega_{p,S}^2 = \omega_{p,S;1}^2 + \omega_{p,S;2}^2$, yielding $\omega_{p,S} \simeq 3570$ cm^{-1}, only somewhat larger than the experimentally-determined value of $\omega_{p,S} \simeq 3280 \pm 200$ cm^{-1}.

The observation of two gap features is consistent with a number of recent theoretical works that propose that isotropic *s*-wave gaps form on the electron and hole pockets but change sign between different Fermi surfaces,[67,68] the so-called $s^{\pm}$ model. However, there is considerable flexibility in this approach that allows for situations in which the sign does not change between the Fermi surfaces (s^{++}), $s^{\pm}$ with nodes on the electron pockets for moderate electron doping, nodeless *d*-wave superconductivity for strong electron doping, as well as nodal *d*-wave superconductivity for strong hole doping.[69] The observation of multiple gaps is also consistent with an ARPES study on this material which observed isotropic gaps on all Fermi surfaces, with $\Delta_1 \simeq 2.5$ meV (hole pocket) and $\Delta_2 \simeq 4.2$ meV (electron pocket).[28] These results are in reasonable agreement with the values determined using our simple model, $\Delta_1 \simeq 2.8$ meV and $\Delta_2 \simeq 5.6$ meV, and the reduction of the conductivity at low frequency for $T \ll T_c$ suggests the absence of nodes. The ARPES study would tend to suggest that the large gap associated with the electron pocket corresponds to the weak, narrow Drude contribution, while the small gap associated with the hole pocket corresponds to the strong, broad Drude response. This is also consistent with our earlier observation of a relatively small scattering rate on the electron pocket in $Fe_{1.03}Te$.[43]

D. Parameter scaling

In our previous study of this material, we noted that it fell on the general scaling line originally observed for the high-temperature superconductors,[36,37] recently demonstrated for some of the iron-based materials,[70] $\rho_{s0}/8 \simeq 4.4\,\sigma_{dc}T_c$, where σ_{dc} is measured just above T_c. A natural consequence of the BCS theory in the dirty limit is the emergence of a similar scaling line[37,71] $\rho_{s0}/8 \simeq 8.1\sigma_{dc}T_c$ (dotted line in Fig. 8). The experimentally-determined values of $\sigma_{dc} \equiv \sigma_1(\omega \rightarrow 0) = 5600 \pm 400$ Ω^{-1}cm^{-1} and $\omega_{p,S} \simeq 3300$ cm^{-1} ($\rho_{s0} \equiv \omega_{p,S}^2$) indicate that this material falls on the scaling line in the vicinity of the underdoped cuprates, as shown in Fig. 8. The decomposition of the superconducting response into two bands allows the different contributions to the superfluid den-

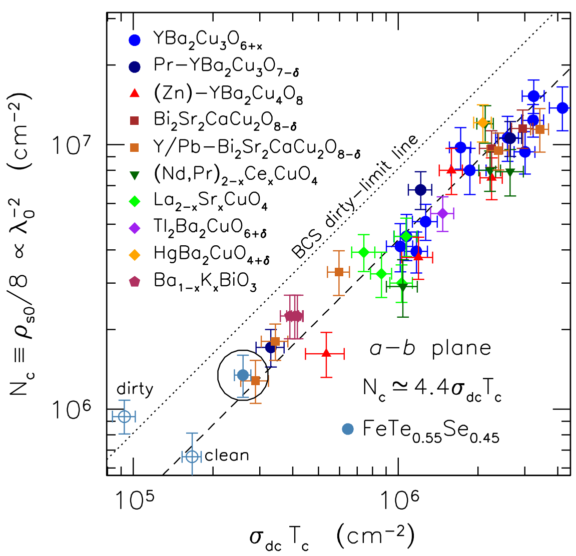

FIG. 8. (Color online) The log-log plot of the in-plane spectral weight of the superfluid density $N_c \equiv \rho_{s0}/8$ vs $\sigma_{dc}\,T_c$, for a variety of electron and hole-doped cuprates compared with the result for $FeTe_{0.55}Se_{0.45}$. The dashed line corresponds to the general result for the cuprates $\rho_{s0}/8 \simeq 4.4\sigma_{dc}T_c$, while the dotted line is the result expected for a BCS dirty-limit superconductor in the weak-coupling limit, $\rho_{s0}/8 \simeq 8.1\,\sigma_{dc}T_c$. The open circles represent the different contributions to the superfluid density in $FeTe_{0.55}Se_{0.45}$; the solid circle is the experimental value.

sity to be examined (Fig. 7). The dirty-limit contribution ($\sigma_{dc} \simeq 2000\ \Omega^{-1}\text{cm}^{-1}$ and $\omega_{p,S} \simeq 2740\ \text{cm}^{-1}$) falls very close to the calculated BCS dirty-limit scaling line, while the clean-limit contribution ($\sigma_{dc} \simeq 3600\ \Omega^{-1}\text{cm}^{-1}$ and $\omega_{p,S} \simeq 2300\ \text{cm}^{-1}$) falls to the right; this latter behavior is expected and has been previously discussed.[37] Initially, it was thought that the materials that fell on the scaling line were likely in the dirty limit.[37] However, it has been shown that many superconducting materials fall on the scaling line, and many of them are not in the dirty limit.[72] Moreover, it has been recently demonstrated that the scaling relation is more robust than originally thought and should be valid for most materials, including those that approach the clean limit,[38] suggesting that the scaling relation is an intrinsic property of the BCS theory of superconductivity. Therefore, even though the contributions to the superfluid density in $FeTe_{0.55}Se_{0.45}$ come from the clean as well as the dirty limit, the material should, and indeed does, fall on the universal scaling line.

IV. CONCLUSIONS

The detailed optical properties of the multiband superconductor $FeTe_{0.55}Se_{0.45}$ ($T_c = 14$ K) have been examined for light polarized in the Fe-Te/Se (a-b) planes for numerous temperatures above T_c, as well as several below. In recognition of the multiband nature of this material, the optical properties are described by the two-Drude model. In the normal state the two-Drude model yields a relatively weak Drude response ($\omega_{p,D;1} \simeq 3000\ \text{cm}^{-1}$) that is quite narrow at low temperature ($1/\tau_{D,1} \simeq 30\ \text{cm}^{-1}$ at 20 K) but which grows quickly with increasing temperature, and a strong Drude response ($\omega_{p,D;1} \simeq 14\,500\ \text{cm}^{-1}$) with a large scattering rate ($1/\tau_{D,2} \simeq 1420\ \text{cm}^{-1}$) that is essentially temperature independent. It is demonstrated that the generalized-Drude model may not be used reliably in multiband materials, except in those cases where chemical substitution has effectively rendered the material either completely electron- or hole-doped. In the superconducting state for $T \ll T_c$ the optical conductivity is reproduced quite well using the normal-state properties for $T \gtrsim T_c$ and Mattis-Bardeen formalism with a small gap ($\Delta_1 \simeq 23\ \text{cm}^{-1}$ or about 2.8 meV) applied to the strong Drude component, and a large gap ($\Delta_2 \simeq 45\ \text{cm}^{-1}$ or about 5.6 meV) applied to the narrow Drude component. Because the scattering rates on the two bands are quite different, this places one band in the dirty limit ($1/\tau \gg \Delta$) and the other close to the clean limit ($1/\tau \lesssim \Delta$), effectively placing this material simultaneously in both the clean and dirty limit. The estimate for the superfluid density of $\rho_{s0} \simeq 3600\ \text{cm}^{-1}$ using this model is quite close to the experimentally-determined value $\rho_{s0} \simeq 3300\ \text{cm}^{-1}$, which places this material on the universal scaling line for high-temperature superconductors in the region of the underdoped cuprates, similar to other iron-based superconductors.

ACKNOWLEDGMENTS

We would like to acknowledge illuminating discussions with L. Benfatto, K. Burch, A. V. Chubukov, J. C. Davis, H. Ding, M. Dressel, Z. W. Lin , H. Miao and S. Uchida. This work is supported by the Office of Science, U.S. Department of Energy under Contract No. DE-SC0012704.

* homes@bnl.gov
† Los Alamos National Laboratory, Center for Integrated Nanotechnologies, MPA-CINT, MS K771, Los Alamos, New Mexico 87545

1 Y. Kamihara, T. Watanabe, M. Hirano, and H. Hosono, J. Am. Chem. Soc. **130**, 3296 (2008).
2 K. Ishida, Y. Nakai, and H. Hosono, J. Phys. Soc. Japan **78**, 062001 (2009).

[3] F.-C. Hsu, J.-Y. Luo, K.-W. Yeh, T.-K. Chen, T.-W. Huang, P. M. Wu, Y.-C. Lee, Y.-L. Huang, Y.-Y. Chu, D.-C. Yan, and M.-K. Wu, Proc. Nat. Acad. Sci. U.S.A. **105**, 14262 (2008).

[4] Z.-A. Ren, J. Yang, W. Lu, W. Yi, X.-L. Shen, Z.-C. Li, G.-C. Che, X.-L. Dong, L.-L. Sun, F. Zhou, and Z.-X. Zhao, EPL **82**, 57002 (2008).

[5] D. C. Johnston, Adv. Phys. **59**, 803 (2010).

[6] W. Bao, Y. Qiu, Q. Huang, M. A. Green, P. Zajdel, M. R. Fitzsimmons, M. Zhernenkov, S. Chang, M. Fang, B. Qian, E. K. Vehstedt, J. Yang, H. M. Pham, L. Spinu, and Z. Q. Mao, Phys. Rev. Lett. **102**, 247001 (2009).

[7] I. A. Zaliznyak, Z. Xu, J. M. Tranquada, G. Gu, A. M. Tsvelik, and M. B. Stone, Phys. Rev. Lett. **107**, 216403 (2011).

[8] I. A. Zaliznyak, Z. J. Xu, J. S. Wen, J. M. Tranquada, G. D. Gu, V. Solovyov, V. N. Glazkov, A. I. Zheludev, V. O. Garlea, and M. B. Stone, Phys. Rev. B **85**, 085105 (2012).

[9] S. Medvedev, T. M. McQueen, I. A. Troyan, T. Palasyuk, M. I. Eremets, R. J. Cava, S. Naghavi, F. Casper, V. Ksenofontov, G. Wortmann, and C. Felser, Nat. Mater. **8**, 630 (2009).

[10] T. J. Liu, J. Hu, B. Qian, D. Fobes, Z. Q. Mao, W. Bao, M. Reehuis, S. A. J. Kimber, K. Prokeš, S. Matas, D. N. Argyriou, A. Hiess, A. Rotaru, H. Pham, L. Spinu, Y. Qiu, V. Thampy, A. T. Savici, J. A. Rodriguez, and C. Broholm, Nat. Mater. **9**, 718 (2010).

[11] J. Zhuang, W. K. Yeoh, X. Cui, X. Xu, Y. Du, Z. Shi, S. P. Ringer, X. Wang, and S. X. Dou, Sci. Rep. **4**, 7273 (2014), conference Proceeding.

[12] M. H. Fang, H. M. Pham, B. Qian, T. J. Liu, E. K. Vehstedt, Y. Liu, L. Spinu, and Z. Q. Mao, Phys. Rev. B **78**, 224503 (2008).

[13] G. F. Chen, Z. G. Chen, J. Dong, W. Z. Hu, G. Li, X. D. Zhang, P. Zheng, J. L. Luo, and N. L. Wang, Phys. Rev. B **79**, 140509(R) (2009).

[14] T. Taen, Y. Tsuchiya, Y. Nakajima, and T. Tamegai, Phys. Rev. B **80**, 092502 (2009).

[15] M. Wu, F. Hsu, K. Yeh, T. Huang, J. Luo, M. Wang, H. Chang, T. Chen, S. Rao, B. Mok, C. Chen, Y. Huang, C. Ke, P. Wu, A. Chang, C. Wu, and T. Perng, Physica C **469**, 340 (2009), superconductivity in Iron-Pnictides.

[16] B. C. Sales, A. S. Sefat, M. A. McGuire, R. Y. Jin, D. Mandrus, and Y. Mozharivskyj, Phys. Rev. B **79**, 094521 (2009).

[17] A. Pourret, L. Malone, A. B. Antunes, C. S. Yadav, P. L. Paulose, B. Fauqué, and K. Behnia, Phys. Rev. B **83**, 020504 (2011).

[18] C. Dong, H. Wang, Z. Li, J. Chen, H. Q. Yuan, and M. Fang, Phys. Rev. B **84**, 224506 (2011).

[19] W. Si, Z.-W. Lin, Q. Jie, W.-G. Yin, J. Zhou, G. Gu, P. D. Johnson, and Q. Li, Appl. Phys. Lett. **95**, 052504 (2009).

[20] S. X. Huang, C. L. Chien, V. Thampy, and C. Broholm, Phys. Rev. Lett. **104**, 217002 (2010).

[21] A. Subedi, L. Zhang, D. J. Singh, and M. H. Du, Phys. Rev. B **78**, 134514 (2008).

[22] F. Chen, B. Zhou, Y. Zhang, J. Wei, H.-W. Ou, J.-F. Zhao, C. He, Q.-Q. Ge, M. Arita, K. Shimada, H. Namatame, M. Taniguchi, Z.-Y. Lu, J. Hu, X.-Y. Cui, and D. L. Feng, Phys. Rev. B **81**, 014526 (2010).

[23] A. Tamai, A. Y. Ganin, E. Rozbicki, J. Bacsa, W. Meevasana, P. D. C. King, M. Caffio, R. Schaub, S. Margadonna, K. Prassides, M. J. Rosseinsky, and F. Baumberger, Phys. Rev. Lett. **104**, 097002 (2010).

[24] S.-H. Lee, G. Xu, W. Ku, J. S. Wen, C. C. Lee, N. Katayama, Z. J. Xu, S. Ji, Z. W. Lin, G. D. Gu, H.-B. Yang, P. D. Johnson, Z.-H. Pan, T. Valla, M. Fujita, T. J. Sato, S. Chang, K. Yamada, and J. M. Tranquada, Phys. Rev. B **81**, 220502 (2010).

[25] E. Ieki, K. Nakayama, Y. Miyata, T. Sato, H. Miao, N. Xu, X.-P. Wang, P. Zhang, T. Qian, P. Richard, Z.-J. Xu, J. S. Wen, G. D. Gu, H. Q. Luo, H.-H. Wen, H. Ding, and T. Takahashi, Phys. Rev. B **89**, 140506 (2014).

[26] P. Zhang, P. Richard, N. Xu, Y.-M. Xu, J. Ma, T. Qian, A. V. Fedorov, J. D. Denlinger, G. D. Gu, and H. Ding, App. Phys. Lett. **105**, 172601 (2014).

[27] K. Nakayama, T. Sato, P. Richard, T. Kawahara, Y. Sekiba, T. Qian, G. F. Chen, J. L. Luo, N. L. Wang, H. Ding, and T. Takahashi, Phys. Rev. Lett. **105**, 197001 (2010).

[28] H. Miao, P. Richard, Y. Tanaka, K. Nakayama, T. Qian, K. Umezawa, T. Sato, Y.-M. Xu, Y. B. Shi, N. Xu, X.-P. Wang, P. Zhang, H.-B. Yang, Z.-J. Xu, J. S. Wen, G.-D. Gu, X. Dai, J.-P. Hu, T. Takahashi, and H. Ding, Phys. Rev. B **85**, 094506 (2012).

[29] K. Okazaki, Y. Ito, Y. Ota, Y. Kotani, T. Shimojima, T. Kiss, S. Watanabe, C. T. Chen, S. Niitaka, T. Hanaguri, H. Takagi, A. Chainani, and S. Shin, Phys. Rev. Lett. **109**, 237011 (2012).

[30] C. Homes, A. Akrap, J. Wen, Z. Xu, Z. Lin, Q. Li, and G. Gu, Phys. Rev. B **81**, 180508 (2010).

[31] A. Pimenov, S. Engelbrecht, A. M. Shuvaev, B. B. Jin, P. H. Wu, B. Xu, L. X. Cao, and E. Schachinger, New J. Phys. **15**, 013032 (2013).

[32] A. Perucchi, B. Joseph, S. Caramazza, M. Autore, E. Bellingeri, S. Kawale, C. Ferdeghini, M. Putti, S. Lupi, and P. Dore, Supercond. Sci. Technol. **27**, 125011 (2014).

[33] S. J. Moon, C. C. Homes, A. Akrap, Z. J. Xu, J. S. Wen, Z. W. Lin, Q. Li, G. D. Gu, and D. N. Basov, Phys. Rev. Lett. **106**, 217001 (2011).

[34] D. Wu, N. Barišić, P. Kallina, A. Faridian, B. Gorshunov, N. Drichko, L. J. Li, X. Lin, G. H. Cao, Z. A. Xu, N. L. Wang, and M. Dressel, Phys. Rev. B **81**, 100512(R) (2010).

[35] E. van Heumen, Y. Huang, S. de Jong, A. B. Kuzmenko, M. S. Golden, and D. van der Marel, EPL **90**, 37005 (2010).

[36] C. C. Homes, S. V. Dordevic, M. Strongin, D. A. Bonn, R. Liang, W. N. Hardy, S. Komiya, Y. Ando, G. Yu, N. Kaneko, X. Zhao, M. Greven, D. N. Basov, and T. Timusk, Nature (London) **430**, 539 (2004).

[37] C. C. Homes, S. V. Dordevic, T. Valla, and M. Strongin, Phys. Rev. B **72**, 134517 (2005).

[38] V. G. Kogan, Phys. Rev. B **87**, 220507 (2013).

[39] C. C. Homes, M. Reedyk, D. A. Crandles, and T. Timusk, Appl. Opt. **32**, 2976 (1993).

[40] M. Dressel and G. Grüner, *Electrodynamics of Solids* (Cambridge University Press, Cambridge, 2001).

[41] B. Valenzuela, M. Calderón, G. León, and E. Bascones, Phys. Rev. B **87**, 075136 (2013).

[42] P.-H. Lin, Y. Texier, A. Taleb-Ibrahimi, P. Le Fèvre, F. Bertran, E. Giannini, M. Grioni, and V. Brouet, Phys. Rev. Lett. **111**, 217002 (2013).

[43] Y. M. Dai, A. Akrap, J. Schneeloch, R. D. Zhong, T. S. Liu, G. D. Gu, Q. Li, and C. C. Homes, Phys. Rev. B **90**, 121114 (2014).

[44] K. Umezawa, Y. Li, H. Miao, K. Nakayama, Z.-H. Liu, P. Richard, T. Sato, J. He, D.-M. Wang, G. Chen, H. Ding,

T. Takahashi, and S.-C. Wang, Phys. Rev. Lett. **108**, 037002 (2012).
[45] I. Tsukada, M. Hanawa, S. Komiya, A. Ichinose, T. Akiike, Y. Imai, and A. Maeda, Physica C **471**, 625 (2011), the 23rd International Symposium on Superconductivity.
[46] L. Benfatto and E. Cappelluti, Phys. Rev. B **83**, 104516 (2011).
[47] G. A. Thomas, J. Orenstein, D. H. Rapkine, M. Capizzi, A. J. Millis, R. N. Bhatt, L. F. Schneemeyer, and J. V. Waszczak, Phys. Rev. Lett. **61**, 1313 (1988).
[48] J. Tu, C. Homes, G. Gu, D. Basov, and M. Strongin, Phys. Rev. B **66**, 144514 (2002).
[49] D. N. Basov and T. Timusk, Rev. Mod. Phys. **77**, 721 (2005).
[50] J. W. Allen and J. C. Mikkelsen, Phys. Rev. B **15**, 2952 (1977).
[51] A. Puchkov, D. N. Basov, and T. Timusk, J. Phys.: Condens. Matter **8**, 10049 (1996).
[52] J. P. Carbotte, E. Schachinger, and D. N. Basov, Nature (London) **401**, 354 (1999).
[53] S. Dordevic, C. Homes, J. Tu, T. Valla, M. Strongin, P. Johnson, G. Gu, and D. Basov, Phys. Rev. B **71**, 104529 (2005).
[54] L. Benfatto, E. Cappelluti, L. Ortenzi, and L. Boeri, Phys. Rev. B **83**, 224514 (2011).
[55] R. A. Ferrell and R. E. Glover, III, Phys. Rev. **109**, 1398 (1958).
[56] M. Tinkham and R. A. Ferrell, Phys. Rev. Lett. **2**, 331 (1959).
[57] H. Kim, C. Martin, R. T. Gordon, M. A. Tanatar, J. Hu, B. Qian, Z. Q. Mao, R. Hu, C. Petrovic, N. Salovich, R. Giannetta, and R. Prozorov, Phys. Rev. B **81**, 180503 (2010).
[58] P. K. Biswas, G. Balakrishnan, D. M. Paul, C. V. Tomy, M. R. Lees, and A. D. Hillier, Phys. Rev. B **81**, 092510 (2010).
[59] T. Klein, D. Braithwaite, A. Demuer, W. Knafo, G. Lapertot, C. Marcenat, P. Rodière, I. Sheikin, P. Strobel, A. Sulpice, and P. Toulemonde, Phys. Rev. B **82**, 184506 (2010).
[60] H. Takahashi, Y. Imai, S. Komiya, I. Tsukada, and A. Maeda, Phys. Rev. B **84**, 132503 (2011).
[61] J. J. Tu, G. L. Carr, V. Perebeinos, C. C. Homes, M. Strongin, P. B. Allen, W. N. Kang, E.-M. Choi, H.-J. Kim, and S.-I. Lee, Phys. Rev. Lett. **87**, 277001 (2001).
[62] W. Zimmermann, E. Brandt, M. Bauer, E. Seider, and L. Genzel, Physica C **183**, 99 (1991).
[63] K. Kamarás, S. L. Herr, C. D. Porter, N. Tache, D. B. Tanner, S. Etemad, T. Venkatesan, E. Chase, A. Inam, X. D. Wu, M. S. Hegde, and B. Dutta, Phys. Rev. Lett. **64**, 1692 (1990).
[64] E. G. Maksimov, A. E. Karakozov, B. P. Gorshunov, A. S. Prokhorov, A. A. Voronkov, E. S. Zhukova, V. S. Nozdrin, S. S. Zhukov, D. Wu, M. Dressel, S. Haindl, K. Iida, and B. Holzapfel, Phys. Rev. B **83**, 140502 (2011).
[65] E. G. Maksimov, A. E. Karakozov, B. P. Gorshunov, E. S. Zhukova, Y. G. Ponomarev, and M. Dressel, Phys. Rev. B **84**, 174504 (2011).
[66] A. E. Karakozov, S. Zapf, B. Gorshunov, Y. G. Ponomarev, M. V. Magnitskaya, E. Zhukova, A. S. Prokhorov, V. B. Anzin, and S. Haindl, Phys. Rev. B **90**, 014506 (2014).
[67] I. I. Mazin, D. J. Singh, M. D. Johannes, and M. H. Du, Phys. Rev. Lett. **101**, 057003 (2008).
[68] A. V. Chubukov, D. V. Efremov, and I. Eremin, Phys. Rev. B **78**, 134512 (2008).
[69] A. Chubukov, Annu. Rev. Condens. Matter Phys. **3**, 57 (2012).
[70] D. Wu, N. Barišić, N. Drichko, P. Kallina, A. Faridian, B. Gorshunov, M. Dressel, L. Li, X. Lin, G. Cao, and Z. Xu, Physica C **470**, S399 (2010), proceedings of the 9th International Conference on Materials and Mechanisms of Superconductivity.
[71] J. L. Tallon, J. R. Cooper, S. H. Naqib, and J. W. Loram, Phys. Rev. B **73**, 180504 (2006).
[72] S. V. Dordevic, D. N. Basov, and C. C. Homes, Sci. Rep. **3**, 1713 (2013).